

Abstract. Oscillations of coronal loops are believed to be the primary cause of the solar corona heating. We study the resonant absorption of MHD waves in magnetized flux tubes with graded densities across the cross section of the tube. Within the approximation that resistive and viscous processes are operative in thin layers surrounding the singularities of the MHD equations, we give the full spectrum of the eigenfrequencies, damping rates, as well as, the eigenfields of the normal MHD modes of the tube. Both surface and body modes are analyzed and the contribution of each class to heating of the corona is commented on.

Key words: Sun – corona: magnetohydrodynamics (MHD) – Sun: magnetic fields – Sun: oscillations

A&A manuscript no.
(will be inserted by hand later)

Your thesaurus codes are:
missing; you have not inserted them

Resonant absorption in dissipative flux tubes

H. Safari¹, S. Nasiri^{1,2}, K. Karami^{1,3,4}, and Y. Sobouti¹

¹ Institute for Advanced Studies in Basic Sciences, Gava Zang, P.O. Box 45195-1159, Zanjan, Iran

² Department of Physics, Zanjan University, Zanjan, Iran

³ Institute for Theoretical Physics and Mathematics, P.O. Box 19395-5531, Tehran, Iran

⁴ Department of Physics, University of Kurdistan, P.O. Box 66177-15175, Sanandaj, Iran
email: hsafary@iasbs.ac.ir; nasiri@iasbs.ac.ir; karami@iasbs.ac.ir; sobouti@iasbs.ac.ir

Received / Accepted

1. Introduction

In typical coronal plasmas, damping rates of resonant MHD waves can be a few orders of magnitude larger than the rates of non-resonant waves. The resonant absorption was first suggested by Ionson (1978) as a mechanism for heating of coronal loops. Since then, much analytical and numerical work has been done on the subject.

Rae and Roberts (1982), investigated both eikonal and differential equation approaches for propagation of MHD waves in inhomogeneous plasmas. Hollweg (1987a,b) considered a dissipative layer of planar geometry to study the resonant absorption of coronal loops. Hollweg (1990) studied the resonant absorption of surface waves in the presence of steady equilibrium flows. Poedts et al. (1989, 1990) developed a finite element code to elaborate on the resonant absorption of Alfvén waves in axially symmetric cylinders.

Davila (1987) and Steinolfson & Davila (1993) did much analytical and numerical work on resonant absorption through resistivity. Ofman et al. (1995) included viscous dissipation in their analysis and concluded that the shear viscosity had the same magnitude as the resistive one. Contribution of the compressional viscosity, however, was found to be insignificant.

Goossens et al. (2002) used the TRACE data of Ofman & Aschwanden (2002) to infer the width of the resonantly absorbing layer for 11 coronal loops. Ruderman & Roberts (2002) did similar analysis with the data of Nakariakov et al. (1999).

Van Doorselaere et al. (2004a) studied the resistive absorption of kink modes of one-dimensional cylindrical models by LEDA (Large-scale Eigenvalue solver for the Dissipative Alfvén spectrum) code. They concluded that when the width of the nonuniform layer was increased, their numerical results differed from those of the analytical approximation by as much as 25%. Van Doorselaere et al. (2004b) investigated the effect of longitudinal curvature on quasi-modes in a toroidal coordinate system representing a typical coronal loop. They found that ideal quasi modes were not much influenced by the curvature.

Karami et al. (2002), (hereafter refereed as paper I), studied the full spectrum of MHD modes of oscillations in zero- β magnetic flux tubes with discontinuous Alfvén speed at tube surface. They showed that the problem is reduced to solving a wave equation for the component of the perturbed magnetic field along the tube axis. They found a lower cutoff for the longitudinal wave numbers along the tube axis and an upper cutoff for the radial wave numbers. They also calculated non resonant viscous and ohmic decay rates for each mode.

In the vicinity of singularity, field gradients are large. Recognizing this, Sakurai et al. (1991a, 1999b) and Goossens et al. (1992, 1995), developed a method to analyze dissipative processes in such vicinities and to neglect them elsewhere. Here we combine the two techniques of paper I and of the connection formulae method of Sakurai et al. (1991a), to obtain the resonant damping rates for the full spectrum of the normal modes of magnetic flux tubes. Equations of motion and of field are introduced and solved in section 2. Thin boundary layer and thin tube approximation is studied in section 3. Thin boundary layer approximation in thick tubes is considered in section 4. Numerical results are given in section 5. Concluding remarks are collected in section 6.

2. Equations of motions

The linearized MHD equations for a zero- β , but resistive and viscous plasma are

$$\frac{\partial \delta \mathbf{v}}{\partial t} = \frac{1}{4\pi\rho} \{(\nabla \times \delta \mathbf{B}) \times \mathbf{B} + (\nabla \times \mathbf{B}) \times \delta \mathbf{B}\} + \frac{\eta}{\rho} \nabla^2 \delta \mathbf{v}, \quad (1)$$

$$\frac{\partial \delta \mathbf{B}}{\partial t} = \nabla \times (\delta \mathbf{v} \times \mathbf{B}) + \frac{c^2}{4\pi\sigma} \nabla^2 \delta \mathbf{B}, \quad (2)$$

where $\delta \mathbf{v}$ and $\delta \mathbf{B}$ are the Eulerian perturbations in the velocity and the magnetic fields; ρ , σ , η and c are the mass density, the electrical conductivity, the viscosity and the speed of light, respectively. The simplifying assumptions are:

- Under coronal conditions gas pressure is negligible (zero- β).

- Density scale heights are much larger than the dimensions of flux tube, so that the gravity stratification is negligible.
- Tube geometry is a circular cylinder with cylindrical coordinates, (r, ϕ, z) .
- There is a constant magnetic field along the z axis, $\mathbf{B} = B\hat{z}$.
- The mean density is a function of r only, $\rho(r)$.
- There is no initial steady flow inside or outside of the tube.
- Viscous and resistive coefficients, η , and σ are constants.

For a variable density, $\rho(r)$, a singularity develops wherever the local Alfvén frequency becomes equal to the global frequency of the mode. The relevant radial wave number vanishes and the resonant absorption takes place. Let us denote the radius of the tube by R and a radius beyond which the resonance occurs by $R_1 < R$. The thickness of the resonant layer, $a = R - R_1$, will be assumed to be thin and will be arbitrarily taken to be of the order $R/10$. The choice of density profile is also arbitrary. We will assume constant densities in regions interior to R_1 and exterior to R . And a linear decrease in $R_1 < r < R$. Thus:

$$\begin{aligned}
\rho &= \rho_i, & r &\leq R_1 \\
&= \frac{\rho_i - \rho_e}{R - R_1}[R - r] + \rho_e, & R_1 &\leq r \leq R \\
&= \rho_e < \rho_i, & R &\leq r < \infty.
\end{aligned} \tag{3}$$

The plan is the following:

- In $r < R_1$ and $R < r$, viscosity and resistivity will be ignored and solutions of Eqs. (1) and (2) will be taken from paper I.
- In $R_1 < r < R$, within which the singularity occurs, viscosity and resistivity will be restored and solutions will be found by expanding Eqs. (1) and (2) about the singular point.
- Finally, interior and exterior solutions will be connected with those of the resonant layer by connection formulae of Sakurai et al. (1991a)

2.1. Interior and exterior solutions

From Karami et al, in the absence of dissipation, all three components of $\delta\mathbf{v}$ and the transverse components of $\delta\mathbf{B}$ are expressible in terms of δB_z only. The latter, in turn, is the solution of a second order differential equation. Thus,

$$\frac{k^2}{r} \frac{d}{dr} \left[\frac{r}{k^2} \frac{d\delta B_z}{dr} \right] + \left(k^2 - \frac{m^2}{r^2} \right) \delta B_z = 0, \tag{4}$$

$$\delta B_r = \frac{ik_z}{k^2} \frac{d\delta B_z}{dr}, \quad \delta B_\phi = -\frac{mk_z}{k^2} \frac{\delta B_z}{r}, \tag{5}$$

$$\delta v_r = -\frac{i}{k^2} \frac{\omega}{B} \frac{d\delta B_z}{dr}, \quad \delta v_\phi = \frac{m}{k^2} \frac{\omega}{B} \frac{\delta B_z}{r}, \quad \delta v_z = 0, \tag{6}$$

where $k^2 = \omega^2/v_A^2 - k_z^2$, and $v_A(r) = B/\sqrt{4\pi\rho(r)}$ is the local Alfvén speed. Here we have assumed an exponential ϕ -, z - and t - dependence, $\exp[i(m\phi + k_z z - \omega t)]$ for any component of $\delta\mathbf{v}$ and $\delta\mathbf{B}$.

In the interior region, $r \leq R_1$, solutions of Eq. (4) are

$$\delta B_z = \begin{cases} I_m(k_i r), & k_i^2 < 0, \quad \text{surface waves,} \\ J_m(k_i r), & k_i^2 > 0, \quad \text{body waves,} \quad k_i^2 = \omega^2/v_{A_i}^2 - k_z^2, \end{cases} \quad (7)$$

where J_m and I_m are Bessel and modified Bessel functions of first kind, respectively. In the exterior region, $r \geq R$, the waves should be evanescent. Solutions are

$$\delta B_z = K_m(k_e r), \quad k_e^2 = k_z^2 - \omega^2/v_{A_e}^2 > 0, \quad (8)$$

where K_m is the modified Bessel function of second kind.

2.2. Resonant layer solution

Let $R_1 < r_A < R$ be the radius at which the singularity occurs:

$$k^2(r_A) = \omega^2/v_A^2(r_A) - k_z^2 = 0. \quad (9)$$

Denote $s = r - r_A$, and expand $k^2(r)$ and Eq. (4) about r_A :

$$k^2(r) = -k_z^2 \left[\frac{1}{v_A^2} \frac{dv_A^2}{ds} \right]_{s=0} s, \quad (10)$$

$$\frac{d}{ds} \left[\frac{1}{s} \frac{d\delta B_z}{ds} \right] - \frac{m^2}{r_A^2} \frac{1}{s} \delta B_z = 0. \quad (11)$$

Equation (11) immediately integrates into

$$\delta B_z = c_1 s I_1 \left(\frac{m}{r_A} s \right) + c_2 s K_1 \left(\frac{m}{r_A} s \right). \quad (12)$$

Substituting Eqs. (10) and (12) in Eq. (6) gives

$$\delta v_r = d_1 I_0 \left(\frac{m}{r_A} s \right) + d_2 K_0 \left(\frac{m}{r_A} s \right), \quad (13)$$

where c_1 , c_2 , d_1 and d_2 are constants. The other components of $\delta\mathbf{B}$ and $\delta\mathbf{v}$ are given in Appendix A.

From the behavior of Bessel's functions at $s = 0$, we note that, very close to the singularity, δB_z is constant and δv_r has a logarithmic divergence. In the presence of dissipations, δB_z still remains constant across the singularity. The logarithmic singularity of δv_r , however, reduces to a large but finite jump across the boundary layer. The general form of jump conditions as given by Sakurai et al (1991a), Goossens et al (1992, 1995), Erdélyi et al. (1995), are

$$[\delta B_z] = 0, \quad (14)$$

$$[\delta v_r] = -\pi\tilde{\omega} \frac{1}{|\Delta|} \frac{m^2}{\rho(r_A)r_A^2} B_z \delta B_z, \quad (15)$$

where $\Delta = \frac{d}{dr}(k^2)|_{r_A}$, $\tilde{\omega} = \omega + i\gamma$, ω is the normal mode frequency and γ is the damping rate of oscillations.

To get the dispersion relation, we substitute Eqs (7) and (8) in (14) and (15). For body waves we obtain

$$[\delta B_z] = A_2 K_m(|k_e|R) - A_1 J_m(|k_i|R_1) = 0, \quad (16)$$

$$\begin{aligned}
[\delta v_r] &= -A_2 \frac{i\tilde{\omega} B_z}{k_e^2} \frac{dK_m(|k_e|R)}{dr} - A_1 \frac{i\tilde{\omega} B_z}{k_i^2} \frac{dJ_m(|k_i|R_1)}{dr}, \\
&= -A_1 \pi \tilde{\omega} \frac{1}{|\Delta|} \frac{m^2}{\rho(r_A) r_A^2} B_z J_m(|k_i|R_1).
\end{aligned} \tag{17}$$

Eliminating the constant A_1 and A_2 between Eqs. (16) and (17), gives the complex dispersion relation

$$d_0(\tilde{\omega}, m) + d_1(\tilde{\omega}, m) = 0, \tag{18}$$

where

$$d_0(\tilde{\omega}, m) = -\frac{1}{k_e} \frac{K'_m(|k_e|R)}{K_m(|k_e|R)} - \frac{1}{k_i} \frac{J'_m(|k_i|R_1)}{J_m(|k_i|R_1)}, \tag{19}$$

$$d_1(\tilde{\omega}, m) = -i\pi \frac{1}{|\Delta|} \frac{m^2}{\rho(r_A) r_A^2}, \tag{20}$$

and " ' " on J_m and K_m indicates derivatives with respect to their arguments. Note that Eq. (18) is not a separation of a complex expression into its real and imaginary parts, as $\tilde{\omega}$ itself is a complex one. From Cramer (2001), the damping rate, γ , is given by

$$\gamma = -\frac{\text{Im}d_1(\tilde{\omega}, m)}{\partial d_0(\tilde{\omega}, m)/\partial \tilde{\omega}} \Big|_{\tilde{\omega}=\omega}. \tag{21}$$

The result for surface waves are the same as Eqs. (16)- (21), expect that J_m is replaced by I_m everywhere. This completes the formal solutions of $\tilde{\omega}$ and γ . In the following section we reduce the expressions for dispersion relation and decay rates for certain simplified cases of actual occurrence.

3. Thin tube and thin boundary (TTTB) approximation

With thin tube we mean small tube radius compared with the radial wavelength, i. e., $kR \ll 1$. With thin boundary layer we mean $a/R = (R - R_1)/R \ll 1$. These constraints implies, $k_i \approx k_e$, $r_A \approx R$, $d_0(\omega, m) \approx 0$, and $d_1(\tilde{\omega}, m) \ll d_0(\tilde{\omega}, m)$. Furthermore, for a given k_z and m there is only one of each type of surface and body waves.

For $m \geq 1$, $d_0(\omega, m) = 0$ gives

$$\omega = k_z \sqrt{\frac{2}{\rho_i + \rho_e}}. \tag{22}$$

From Eq. (21) one then gets

$$\gamma = \left\{ \pi \frac{m^2}{|\Delta|} \frac{1}{\rho(r_A) r_A^2} \right\} / \left\{ -\frac{2m\omega\rho_e}{Rk_e} - \frac{2m\omega\rho_i}{Rk_i} \right\} = -\frac{m\omega\pi}{8} \frac{a}{R} \frac{\rho_i - \rho_e}{\rho_e + \rho_i}. \tag{23}$$

Equations (22) and (23) are valid for both surface and body waves; for the behavior of J_m and I_m at small arguments are the same. The damping rate of Eq. (23) is proportional to m , to the inhomogeneity length a/R , and the density contrast $(\rho_i - \rho_e)/(\rho_i + \rho_e)$, in agreement with the findings of Van Doorselaere et al. (2004a).

Thin flux tubes are studied in ample details by Ionson (1978), Wentzel (1979a,b), Wilson (1979, 1980), Edwin & Roberts (1983), Roberts et al. (1984), Hasan & Sobouti (1987), Nasiri (1992), and Nakariakov et al. (1999). Steinolfson & Davila (1993), Karami et al. (2002).

4. Thin boundary approximation

Here, we relax the condition $kR \ll 1$ and keep $a/R \ll 1$. The Bessel functions J_m and I_m behave differently at the boundary. Therefore, the surface and body waves exhibit differences. For a given m and k_z , there is still one surface wave, but a multitude of body waves with different radial wave numbers. A detailed study of the latter waves is given in paper I. There, a trio of wave numbers, (n, m, l) , corresponding to r , ϕ , and z directions, is assigned to each mode. The dispersion relation, the same as $d_0(\omega, m) = 0$ is solved numerically for mode frequencies, ω_{nml} .

From Eq. (21), the damping rate for body waves becomes

$$\begin{aligned} \gamma &= - \left\{ \frac{\pi m^2}{\rho(r_A)r_A^2 |\Delta|} \right\} / \frac{d}{d\omega} \left\{ \frac{1}{k_e} \frac{K'_m(|k_e|R)}{K_m(|k_e|R)} + \frac{1}{k_i} \frac{J'_m(|k_i|R)}{J_m(|k_i|R)} \right\}, \\ &= - \left\{ \frac{\pi m^2}{\omega_{nml}^2 (\rho_i - \rho_e) R^2} \right\} / \frac{d}{d\omega} \left\{ \frac{1}{k_e} \frac{K'_m(|k_e|R)}{K_m(|k_e|R)} + \frac{1}{k_i} \frac{J'_m(|k_i|R)}{J_m(|k_i|R)} \right\}. \end{aligned} \quad (24)$$

Replacing J_m by I_m in Eq. (24) gives the damping rates of surface waves.

A remark on axially symmetric modes: From Eqs. (14) and (15), (A.5) and (A.6), the jumps in δB_z , δv_r , δB_r and δv_z vanish for $m = 0$. From Eqs. (A.2) and (A.3), δB_ϕ and δv_ϕ themselves vanish. One concludes the absence of resonant absorption in such modes. Non resonant absorption will, however, be present. See paper I for relevant rates.

5. Numerical results

As typical parameters for a coronal loop, we adopt radius = 10^3 km, length = 10^5 km, $\rho_e/\rho_i = 0.1$, $\rho_i = 2 \times 10^{-14}$ gr cm $^{-3}$, $B = 100$ G. One finds $v_{A_i} = 2000$ km s $^{-1}$, $v_{A_e} = 6400$ km s $^{-1}$ and $\omega_A = 2$ rad s $^{-1}$.

For body waves, specified by three mode number (n, m, l) , the frequencies, ω_{nml} , the resonant damping rates, γ_{nml} , and the ratios $\gamma_{nml}/\omega_{nml}$, called spectral damping rates, are displayed in Table 1. Only the kink modes, $m = 1$, are considered. The frequencies ω_{nml} are from Paper I. The frequencies increase monotonously with increasing n and/or l . Whereas, the damping rates increase from $l = 1$ up to $[\sim 50]$ and decrease from thereon. The explanation is that for low l 's, wave amplitudes are large near the boundary and in the resonant layer. They shift towards the tube axis as l increases. See Fig.1. This is in contrast with non resonant damping. There, the multitude of different factors so balance each other that damping rates monotonously increase with increasing n and l . See Table 2. In Table 1 spectral damping rates, decrease with increasing n and l . For instance, for $n = 1$ it decreases from 0.0323 for $l = 1$, down to, 0.0024 for $l = 100$. For $n = 2$, they decrease from 0.0001 for $l = 41$ down to 0.00004 for $l = 100$. For a given l there is a similar decrease with increasing n , for example, for $l = 100$, spectral rate decrease from 0.0024 for $n = 1$ to 0.00001 for $n = 3$. This means that modes of higher n and l live

Table 1. Values of ω_{nml} and γ_{nml} for $m = 1$ (kink) body modes with radius = 10^3 km, length = 10^5 km, $B = 100$ G, $\rho_i = 2 \times 10^{-14}$ gr cm $^{-3}$, $\rho_e/\rho_i = 0.1$. Both, frequencies and damping rates, γ_{nml} , are in units of the interior Alfvén frequency, $\omega_A = 2$ rad s $^{-1}$, $R/L = 1/100$ and $a/R = 0.1$. There are no modes in the region of blank entries. The boundary of the blank and filled regions defines the cutoffs of the modes. See paper I for detailed.

l	ω_{nml}			γ_{nml}			$\gamma_{nml}/\omega_{nml}$		
1	0.0434	-	-	0.0014	-	-	0.0323	-	-
2	0.0845	-	-	0.0028	-	-	0.0320	-	-
41	1.5154	4.0473	-	0.0222	0.0004	-	0.0146	0.0001	-
75	2.5957	4.7589	7.4084	0.0132	0.0249	0.0074	0.0051	0.0052	0.0010
100	3.3695	5.3079	7.8652	0.0082	0.0002	0.0001	0.0024	0.00004	0.00001
	$n = 1$	$n = 2$	$n = 3$	$n = 1$	$n = 2$	$n = 3$	$n = 1$	$n = 2$	$n = 3$

longer than those with lower n and l . In the absence of resonance, the case considered in paper I, the situation is different. There, the spectral rates of non resonant damping increases monotonously with increasing n and l . This is because of the fact that, the amplitude of the waves of lower n and l appears to be near the surface in the proximity of the boundary layer.

For surface waves, specified by two mode number (m, l) associated with (ϕ, z) directions, ω_{ml} , γ_{ml} , and γ_{ml}/ω_{ml} are given in table 3, 4, and 5. Both ω 's and γ 's increase with increasing m and/or l . Spectral rates, however, decrease with increasing m and/or l . From table 5, for $m = 1, l = 1$, the spectral damping rate is 0.1027. This means that the corresponding waves will be damped after about 9 oscillations. This is in agreement with findings of Nakariakov et al. (1999) and Goossens et al. (2002) from TRACE data, that indicated ~ 3 or 4 oscillations of flux filaments before they damp out.

The magnetic and velocity components, δB_z and δv_r for body and surface waves of $m = 1$ and 2, are plotted in Figs. 2 to 4. Consistent with the jump conditions of Eqs. (14) and (15), δB_z is continuous but δv_r shows a large jump across the singular point. The jumps in δv_r for both fundamental body and surface modes, $(n, m, l) = (1, 1, 1)$, have the same order of magnitude. The body and surface modes of higher l 's, also show resonance absorption. For them, however, the jump in δv_r is much less pronounced than for the fundamental modes. For $m = 2$, in contrast to $m = 1$, the surface modes play the dominant role.

Table 2. Non resonant damping rates of body waves, α_{nml} , from paper I. Other specifications as in Table 1. Courtesy Karami et al. (2002).

l	ω_{nml}			$\alpha_{nml}(\times 10^{-4})$			$\alpha_{nml}/\omega_{nml} (\times 10^{-4})$		
1	0.0434			0.0001			0.0023		
2	0.0845	-	-	0.0569	-	-	0.6734		
41	1.5154	4.0473		0.1827	1.3035		0.1205	0.3221	
75	2.5957	4.7589	7.4084	0.5361	1.8022	4.3675	0.2065	0.3787	0.5895
100	3.3695	5.3079	7.8652	0.9035	2.2420	4.9228	0.2681	0.4220	0.6258
	$n = 1$	$n = 2$	$n = 3$	$n = 1$	$n = 2$	$n = 3$	$n = 1$	$n = 2$	$n = 3$

Table 3. Surface waves of $m = 1$, $R/L = 1/100$, and $a/R = 0.1$. Other specifications as in Table 1. There is only such mode in radial extent.

l	ω_{ml}	γ_{ml}	γ_{ml}/ω_{ml}
1	0.0423	0.0013	0.0307
2	0.0846	0.0025	0.0295
41	1.6052	0.0301	0.0187
75	2.8782	0.0454	0.0157
100	3.8391	0.0579	0.0151

Table 4. Surface waves of $m = 2$, $R/L = 1/100$, $a/R = 0.1$. Other specifications as in Table 1.

l	ω_{ml}	γ_{ml}	γ_{ml}/ω_{ml}
1	0.0423	0.0025	0.0591
2	0.0847	0.0047	0.0550
41	1.6953	0.0895	0.0527
75	3.0400	0.1425	0.0468
100	4.0211	0.1772	0.0440

Table 5. Surface waves of $m = 1$, $R/L = 1/50$, $a/R = 0.1$ (thick tube thin boundary layer). Other specifications as in Table 1.

l	ω_{ml}	γ_{ml}	γ_{ml}/ω_{ml}
1	0.0789	0.0081	0.1027
2	0.1685	0.0096	0.0290
50	3.8391	0.0578	0.0151
75	5.8451	0.0797	0.0136
100	7.9197	0.0909	0.0115

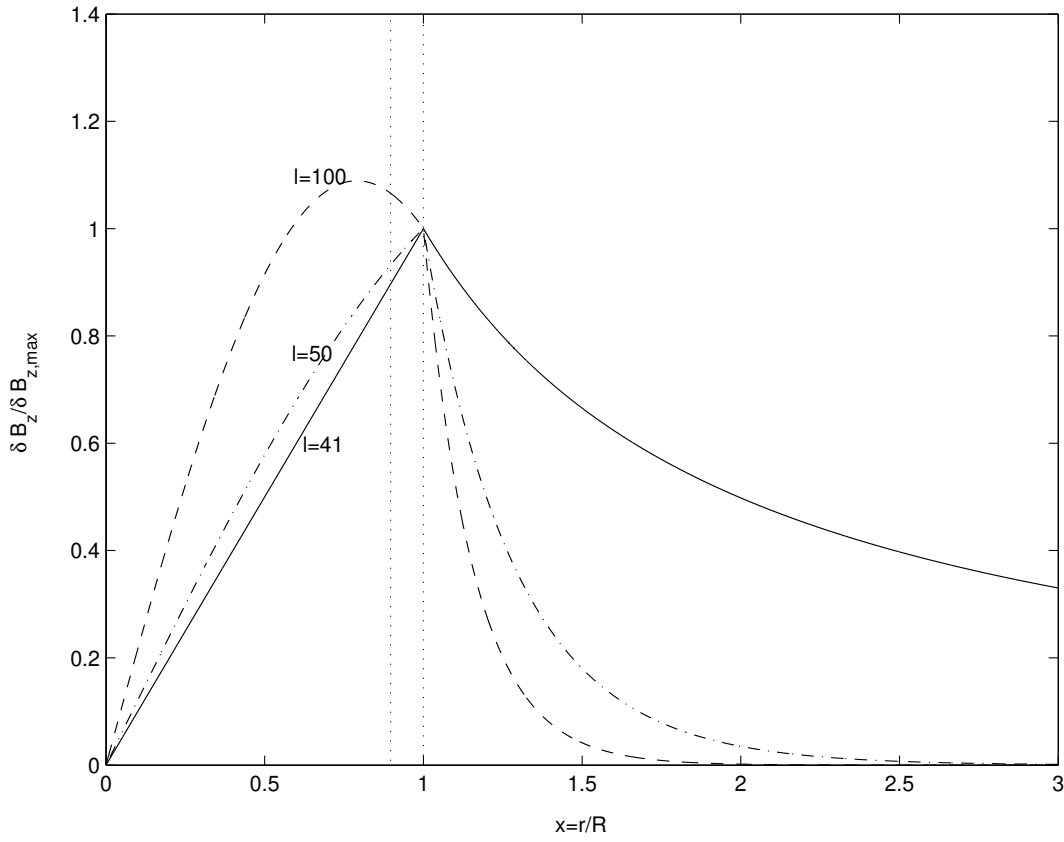


Fig. 1. Magnetic component ($\delta B_z / \delta B_{z,max}$) for $m = 1$ (kink) body modes. $l = 41, 50, 100$. Note that the maximum wave amplitude shifts towards the tube axis as l increases.

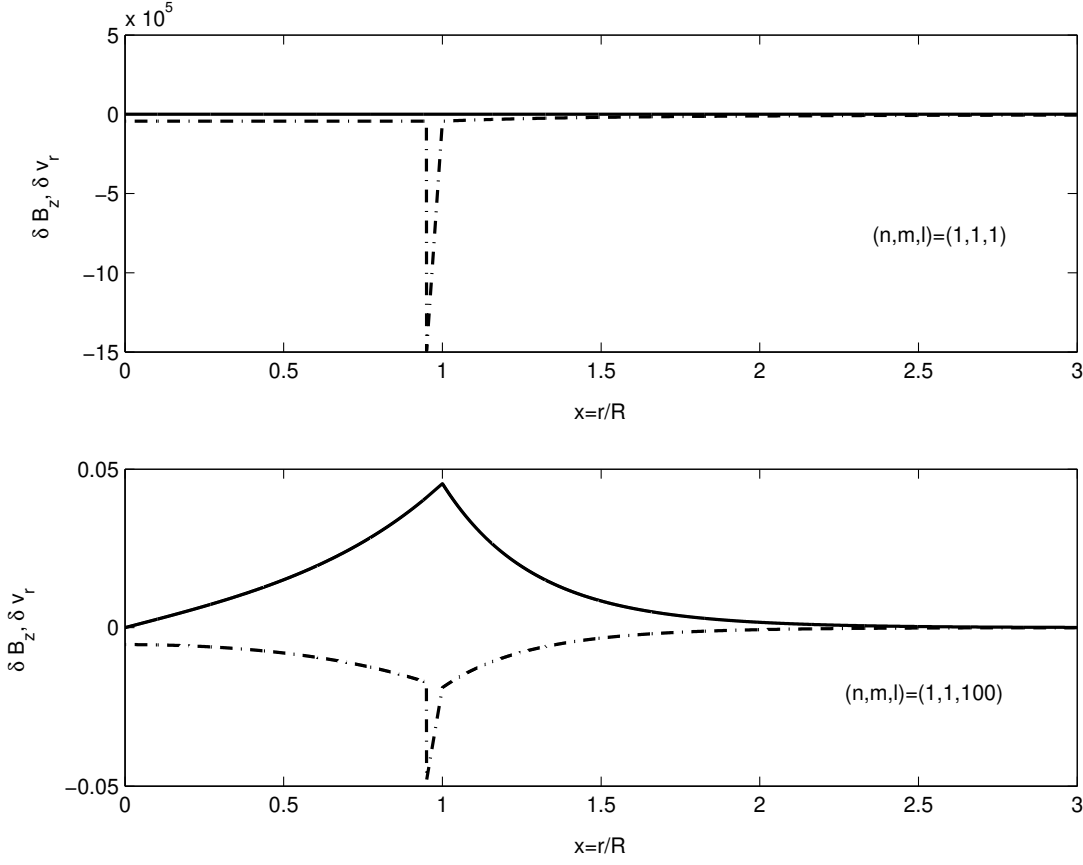


Fig. 2. Magnetic and velocity field components for $m = 1$ (kink) body modes. δB_z solid curves; δv_r dash-dotted curves. Other parameters are: radius = 10^3 km, length = 10^5 km, and $\rho_e/\rho_i = 0.1$.

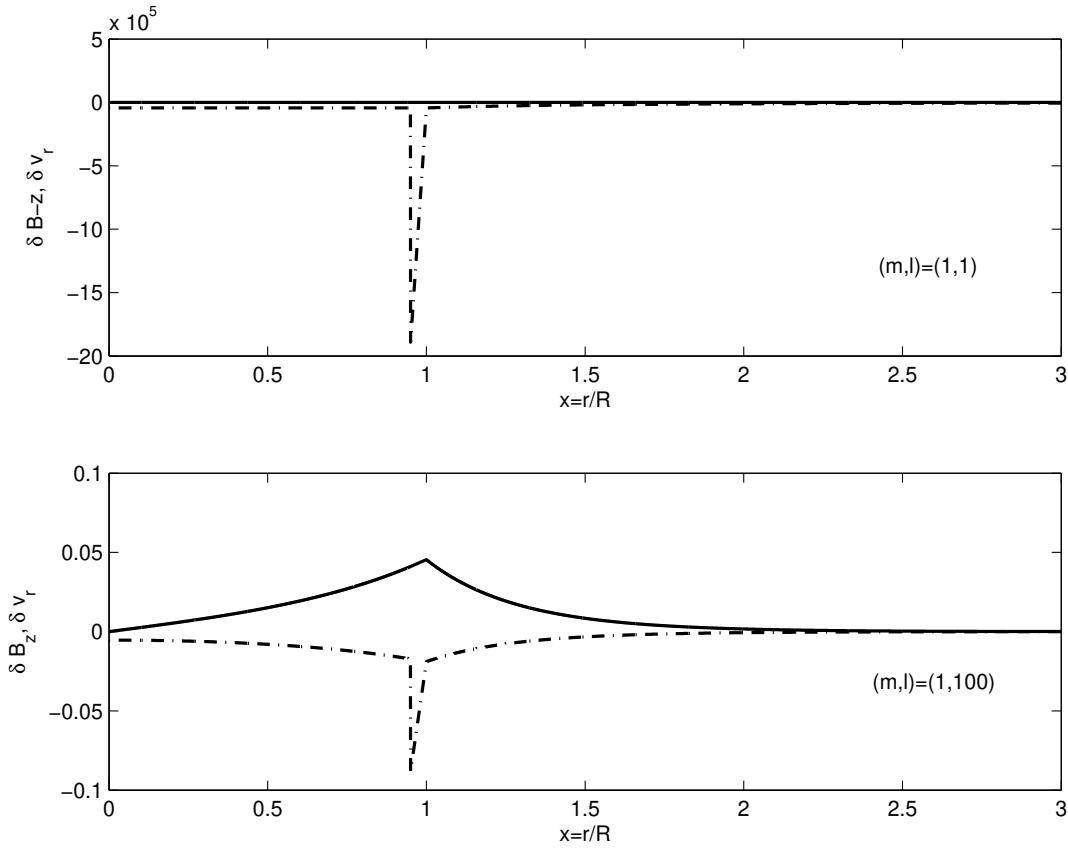


Fig. 3. Same as Fig. 2 for $m = 1$ (kink) surface modes.

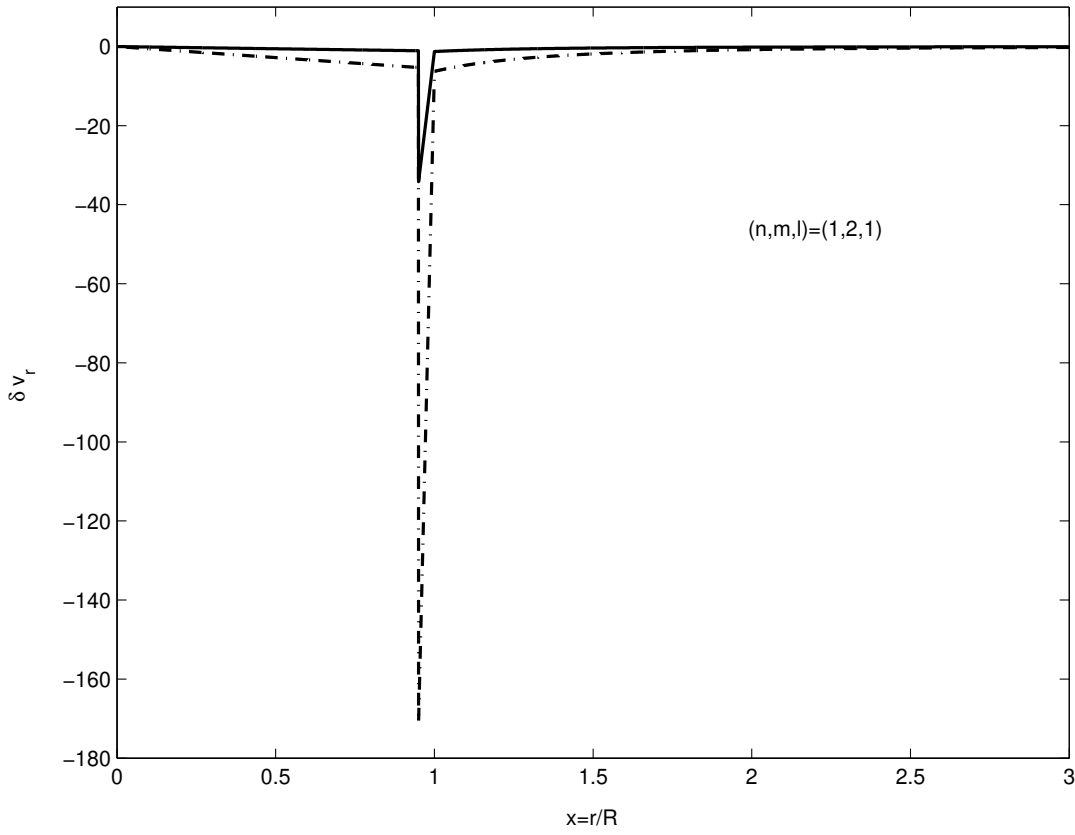


Fig. 4. Same as Fig. 2 for $m = 2$ surface and body modes. Radial component of velocity field, δv_r , body modes (solid curve) and surface modes (dash-dotted curve). The radial number for body mode is $n = 1$.

6. Concluding remarks

We have studied magnetic flux tubes with specified density profiles in the presence of viscous and resistive dissipations. Solutions to singular equations of motion are obtained by connection formulae technique. The full spectrum of the eigenfrequencies, the eigenfields and the damping rates are calculated for body and surface waves. The spectral damping rates decrease by increasing n and l , showing that the fundamental kink mode plays the dominant role in heating of the corona. For $n = 1$, the body and surface waves contribute almost equally to the heating mechanism. However, for $m = 2$ the surface waves are more effective compared with body waves of the same order of n .

By keeping the inhomogeneity length scale, a/R , fixed and increasing the tube length scale, R/L , the damping time scale gets closer to the observed values of TRACE. The behavior of body waves as a function of n and/or l is completely different whether the resonance layer is present or absent.

Acknowledgements. This work was supported by the Institute for Advanced Studies in Basic Sciences (IASBS), Zanjan. The authors wish to thank Prof. Robert Erdélyi and, Marcel Goossens, for valuable consultations.

Appendix A: The remaining components of eigenfields

This is a rewrite of Eqs.(5) and (6) for the boundary layer, within which the resonance take place. Eq. (10) is used to reduce $k^2(r)$ near the resonant radius.

$$\delta B_r = -i \frac{v_A^2(r_A)}{k_z \frac{dv_A^2}{dr} |_{r_A}} \frac{1}{s} \frac{d\delta B_z}{ds}, \quad (\text{A.1})$$

$$\delta B_\phi = \frac{m}{r_A} \frac{v_A^2(r_A)}{k_z \frac{dv_A^2}{dr} |_{r_A}} \frac{\delta B_z}{s}, \quad (\text{A.2})$$

$$\delta v_\phi = -\frac{m\omega}{r_A} \frac{v_A^2(r_A)}{k_z \frac{dv_A^2}{dr} |_{r_A}} \frac{\delta B_z}{s}, \quad (\text{A.3})$$

$$\delta v_z = 0. \quad (\text{A.4})$$

The ϕ - components are singular at $s = 0$. For δB_r and δv_z , the jumps across the boundary layer are

$$[\delta B_r] = -\frac{k_z B_z}{\tilde{\omega}} [\delta v_r], \quad (\text{A.5})$$

$$[\delta v_z] = 0. \quad (\text{A.6})$$

References

- Cramer, N. F. 2001, *The Physics of Alfvén Waves*, (John Wiley & Sons, Inc.), 100
- Davila, J. M. 1987, *ApJ*, 317, 514
- Edwin, P. M., & Roberts, B. 1983, *Sol. Phys.*, 88, 179
- Erdélyi, R., Goossens, M., & Ruderman, M. S. 1995, *Sol. Phys.*, 161, 123
- Goossens, M., Hollweg, J. V., & Sakurai, T. 1992, *Sol. Phys.*, 138, 233
- Goossens, M., Ruderman, M. S., & Hollweg, J. V. 1995, *Sol. Phys.*, 157, 75
- Goossens, M., Andries, J., & Aschwanden, M. J. 2002, *A&A*, 394, L39
- Hasan, S. S., & Sobouti, Y. 1987, *MNRAS*, 228, 427
- Hollweg, J. V. 1987a, *ApJ*, 312, 880
- Hollweg, J. V. 1987b, *ApJ*, 320, 875
- Hollweg, J. V. 1990, *J. Geophys. Res.*, 95, 2319
- Ionson, J. A. 1978, *ApJ*, 226, 650
- Karami, K., Nasiri, S. & Sobouti, Y. 2002, *A&A*, 396, 993 (Paper I)
- Nakariakov, V. M., Ofman, L., Deluca, E. E., Roberts, B., & Davila, J. M. 1999, *Science*, 285, 862
- Nasiri, S. 1992, *A&A*, 261, 615
- Ofman, L., Davila, J. M., & Steinolfson, R. S. 1995, *ApJ*, 444, 471
- Ofman, L., & Aschwanden, M. J. 2002, *ApJ*, 576, L153
- Poedts, S., Goossens, M., & Kerner, W. 1989, *Sol. Phys.*, 123, 83
- Poedts, S., Goossens, M., & Kerner, W. 1990, *ApJ*, 360, 279
- Rae, I. C. & Roberts, B. 1982, *MNRAS*, 201, 1171
- Roberts, B., Edwin, P. M., & Benz, A. O. 1984, *ApJ*, 279, 857
- Ruderman, M. S. & Roberts, B. 2002, *ApJ*, 577, 475
- Sakurai, T., Goossens, M., & Hollweg, J. V. 1991a, *Sol. Phys.*, 133, 247
- Sakurai, T., Goossens, M., & Hollweg, J. V. 1991b, *Sol. Phys.*, 133, 227
- Steinolfson, R. S., & Davila, J. N. 1993, *ApJ*, 415, 354
- Van Doorselaere, T., Andries, J., Poedts, S., & Goossens, M. 2004a, *ApJ*, 606, 1223
- Van Doorselaere, T., Debusscher, A., Andries, J., & Poedts, S. 2004b, *A&A*, 424, 1065
- Wentzel, D. G. 1979a, *ApJ*, 227, 319
- Wentzel, D. G. 1979b, *A&A*, 76, 20
- Wilson, P. R. 1979, *A&A*, 71, 9
- Wilson, P. R. 1980, *A&A*, 87, 121